

## SNOW BIDIRECTIONAL REFLECTANCE MODEL USING NON-SPHERICAL SNOW PARTICLES AND ITS VALIDATION WITH FIELD MEASUREMENTS

*Tomonori Tanikawa<sup>1\*</sup>, Teruo Aoki<sup>2</sup>, Masahiro Hori<sup>3</sup>, Akihiro Hachikubo<sup>4</sup> and Masamu Aniya<sup>1</sup>*

1. Graduate School of Life and Environmental Sciences, University of Tsukuba, Tsukuba, Japan
2. Meteorological Research Institute, Tsukuba, Japan
3. Japan Aerospace Exploration Agency, Tokyo, Japan
4. New Energy Resources Research Center, Kitami Institute of Technology, Kitami, Japan

### ABSTRACT

Radiative transfer models, using non-spherical snow particles, were developed to examine the effect of snow grain shape on the angular distribution of snow reflectance. To represent the natural ice crystals, surface roughness is added to the ray-tracing calculation in the single-scattering calculation. For validation of the radiative transfer model, we compared the simulated angular distribution of the reflectance with the observed one. For the new snow, the comparison between the simulated results using cylindrical ice particles with rough surface and the observed ones show good agreement for any viewing angle. For granular snow, the simulated results using ellipsoids in the visible region are consistent with the observed ones while in the near-infrared region the angular distribution of the reflectance is approximately simulated. The angular distribution of the reflectance depends on the snow grain shape and the surface roughness of ice crystals, and on the surface roughness providing a smooth reflectance pattern. Radiative transfer models of snow using non-spherical particles with rough surface are more suitable than those of snow using spherical particles for the calculation of the angular distribution of the reflectance.

**Keywords:** radiative transfer model of snow, HDRF, non-spherical particle, surface roughness.

### INTRODUCTION

Remote sensing, using visible and near-infrared wavelengths, is one of the most suitable techniques for monitoring snow physical parameters at regional and global scales. However, it is difficult to analyse remote sensing data of flat snowfields, because the satellite sensor collects only a small portion of the energy which is reflected over all directions from the surface. The assumption of isotropic reflectance of snow is too simple to retrieve the snow physical parameters; the results of which may contain large errors due to the strong anisotropic reflectance of the snow surface (e.g. 1,2). Knowledge of the angular distribution of snow reflectance is, therefore, a crucial factor in accurately retrieving snow physical parameters from remote sensing data.

Various studies have focused on measuring the angular distribution of snow reflectance (e.g. 1,3,4). These studies show the anisotropic reflection properties of snow. At several Antarctic sites the hemispherical- directional reflectances at four wavelengths were examined (5). The effects of snow grain-size and type on the hemispherical-directional reflectance from optical measurements were demonstrated (6). Recently, improving the performance of spectrometry and goniometry has given us in-depth information of the angular dependence of snow and ice reflectance (1,3,4,7,8). These measurements address the dependence on the hemispherical-directional reflectances to snow grain size, type and solar zenith and azimuth angle, reflected angle, explored at high angular and spectral resolutions. However, measurements of the angular distribution of snow reflectance are required

---

\* Now with Snow and Ice Research Laboratory, Department of Civil Engineering, Kitami Institute of Technology, Kitami, Hokkaido, 090-8507, Japan; [tanikawa\(at\)mail.kitami-it.ac.jp](mailto:tanikawa(at)mail.kitami-it.ac.jp)

under various snow conditions with high angular and spectral resolutions and under geometric conditions, because natural snow surface conditions show wide variation.

On the other hand, in most of the remote sensing algorithms for retrieving snow physical parameters, the shape of a snow grain is assumed to be a sphere in the single-scattering calculations, although ice crystals have a wide range of different shapes (e.g. 2,9,10,11). This is because spheres are three-dimensional which makes it easy to define their grain size. However, there are some disadvantages of using spherical particles in the single-scattering calculation; the rainbow patterns of reflectance are inadvertently simulated although there is no rainbow pattern in the observed reflectance (1,4); and the single-scattering properties are different between spherical and non-spherical particles (e.g. 12). The simulated hemispherical-directional reflectances using the hexagonal ice plate as surrogate for snow particles are roughly consistent with the observed ones (3). However, it is not clear if the hexagonal ice plate is applicable to all snow types. A snow shape with a smooth phase function is suitable for the calculation of the hemispherical-directional reflectances (1). For developing an algorithm to accurately retrieve snow physical parameters, radiative transfer models of snow using non-spherical particles with smooth phase functions corresponding to each snow grain are necessary.

The purpose of this study is to examine the effect of the snow grain shape on the angular distribution of reflectance of snow, using spectral data, snow pit work data and radiative transfer models. To achieve this, we measured the spectral hemispherical-directional reflectance factor (*HDRF*) for new and old snow in a flat snowfield. The theoretically calculated *HDRFs* using the developed radiative transfer models are compared with the measured ones for the two types of snow.

## OBSERVATION CONDITIONS AND HDRF MEASUREMENTS

The *HDRF* observations were carried out for new snow in February 2001 and for old snow during the melting season in March 2004 in Hokkaido, Japan. For the new snow, the snow surface was covered by dendrites and second layers, which mainly consisted of faceted crystals and depth hoar. Most of the old snow layers consisted of granular snow and the snow surface was partially covered by sun crust (melt freeze crust). The snow grain size (radius) was measured with a resolution of about 10  $\mu\text{m}$  using a handheld lens employing the same method as described in (1). There were two kinds of grain size dimensions: one-half of diameters of major axis of crystals or dendrites ( $r_1$ ); and one-half of branch of dendrites or one-half of dimensions of the narrower portion of broken crystals ( $r_2$ ). For the new snow, the snow grain sizes  $r_1$  and  $r_2$  in the uppermost 2 cm layer were 100–1000  $\mu\text{m}$  and 30–50  $\mu\text{m}$ , respectively, and those below 2 cm were 250–500  $\mu\text{m}$  and 100–200  $\mu\text{m}$ , respectively. Regarding the old snow, the first layer consisted of the snow grains of  $r_1 = 500\text{--}2000 \mu\text{m}$  and  $r_2 = 100\text{--}500 \mu\text{m}$  and the layer from the surface to 3 cm depth was granular snow where  $r_1 = 1000\text{--}3000 \mu\text{m}$  and  $r_2 = 400\text{--}1000 \mu\text{m}$ .

The observations were made using a grating spectrometer, FieldSpec Pro FR (ASD Inc., USA), with a pointing system for snow surface. The pointing system is for observing the same snow surface from any viewing angle (Figure 1). The reflected light from the snow surface is taken into the spectrometer by foreoptics with a 3° field of view, and an optical fibre. Although the foreoptics keeps its pointing to the same snow surface from any viewing angle, the precise area of the measured snow surface varies with the viewing angle. The area is circular for nadir observations and changes to an ellipse for non-nadir observations. However, smoother reflection functions could be obtained with this system than with the optical system used as described in (1). In the *HDRF* measurements, downward solar flux measurements at the snow surface are necessary. Since the downward solar flux was difficult to measure accurately, a white reference standard (WRS) of SRT-99 (Labsphere Inc., USA) was used. The *HDRF* we present here is defined by

$$HDRF(\theta_o, \theta_v, \Delta\phi) = \frac{\pi I(\theta_v, \Delta\phi)}{\cos\theta_o F_o + F_d}$$

where  $I$  is the upward radiance reflected from the surface,  $F_o$  is the direct solar irradiance for the surface that is perpendicular to the sun, and  $F_d$  is the diffuse solar irradiance.  $(\theta_o, \theta_v)$  is the solar zenith and reflected angle,  $\Delta\phi$  is the relative azimuth angle.

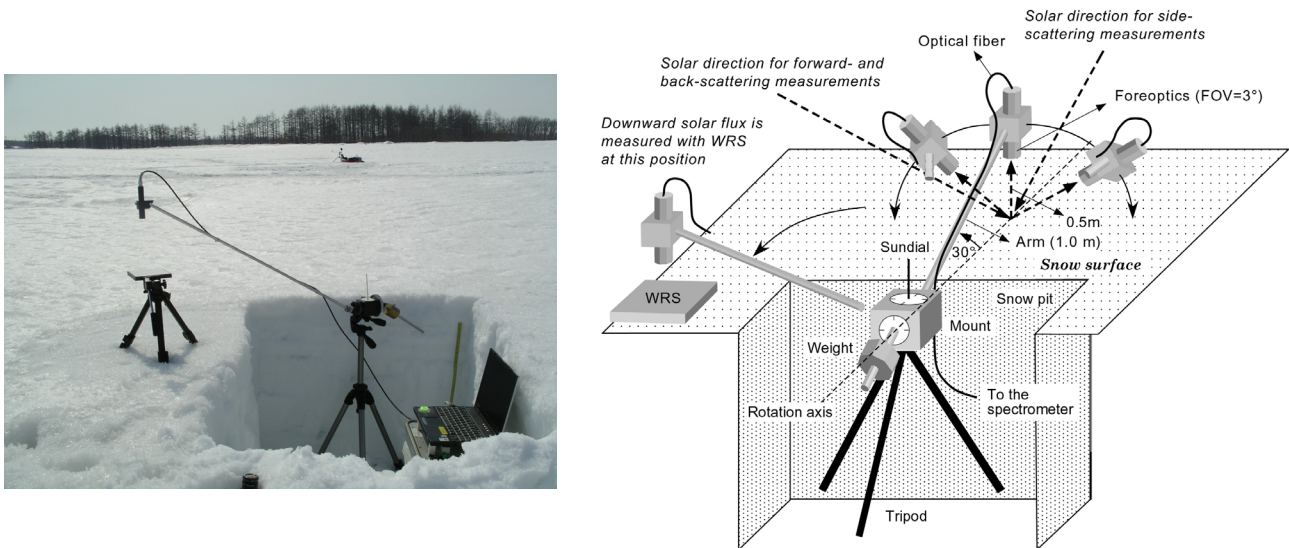


Figure 1: (left) Photograph of the observational setup, and (right) schematic illustration of the setup for upward radiance and downward solar flux measurements. The downward solar flux was observed by directing the optical fibre tip of the spectrometer to the upper surface of the white reference standard (WRS) placed on a tripod on the snow surface. The upward radiance was directly measured by the optical fibre.

### RADIATIVE TRANSFER MODEL

A multiple-scattering radiative transfer model for the atmosphere-snow system was used for calculating the angular distribution of reflectance (1) and was used to compare the theoretically calculated *HDRF* with the observed one. The radiative transfer model is based on the doubling and adding method for multiple scattering (13). Single-scattering parameters are calculated by a ray-tracing technique (14). Snow grain shapes are assumed to be cylindrical for new snow and ellipsoidal for old snow. The reason for using the cylinders for the new snow is as follows: the single-scattering properties of the dendrites show that the branch shape and size are more important than the effects of the entire snow crystal shape (15,16). Furthermore, the optically equivalent grain size is not the size of the entire snow crystal but the branch width of an individual particle (1). The cylinder is suitable as surrogate for the branch of the dendrite (17) and is therefore used in the model. . On the other hand, for old snow, we use spheroids instead of spheres for granular snow, because rainbow patterns of reflectance are almost absent in the snow surface (1,4), and an optically equivalent grain size for granular grains is not the dimension of the cluster but each grain's diameter (1).

For representing natural ice crystals in the calculation, we applied surface roughness to the single-scattering calculation. When a ray hits a crystal surface, the normal direction to the surface is tilted with respect to its original direction by a certain angle. This tilt angle is specified by a 2-D Gaussian distribution (16) and is given by

$$P(Z_x, Z_y) = \frac{1}{\pi\sigma^2} \exp\left(-\frac{Z_x^2 + Z_y^2}{\sigma^2}\right)$$

where  $Z_x$  and  $Z_y$  are the tilt defined for a facet of rough surface along orthogonal directions,  $\sigma$  is a parameter determining the magnitude of roughness, in which  $\sigma = 0-0.005$ ,  $0.005-0.05$ ,  $0.05-0.2$  correspond to slight, moderate, and deep roughness in the single-scattering calculation, respectively (16).

Figure 2 shows the phase function of cylindrical and ellipsoidal ice particles. The aspect ratio of the cylindrical ice particles is set to  $2R/L = 0.1$  ( $R$  is the base radius, and  $L$  is the length) as column-like cylinder, because the single-scattering properties are similar when set to long enough column-like cylinders. For ellipsoidal ice particles, the aspect ratio is set to  $a/c = 0.1$ , i.e. as a prolate because there is no rainbow for  $a/c > 1/3$ ;  $a$  and  $c$  are the length of the crystal's  $a$ - and  $c$ -axis, respectively, and the length of the  $a$ -axis is the same as that of  $b$ -axis. The size of non-spherical ice particles can be represented by the equivalent  $V/A$ -sphere (12). Phase functions for cylindrical ice particles  $r_{VA} = 50 \mu\text{m}$  at  $\lambda = 0.55 \mu\text{m}$  and  $1.64 \mu\text{m}$  are shown in Figure 2a. In the case of  $\sigma = 0.0$ , peaks at  $\theta = 46^\circ$ ,  $135^\circ$  and  $180^\circ$  were simulated. The halo peak at  $\theta = 46^\circ$  is caused by the minimum deviation at the  $90^\circ$  ice prisms (18), but is not the primary halo. When  $\sigma = 0.0$ , the backscattering peak at  $\theta = 180^\circ$  caused by the rays internally reflected by mutually perpendicular faces (side- and end-faces) (18). Some peaks ( $\theta = 46^\circ$ ,  $135^\circ$ , and  $180^\circ$ ) vanish and are replaced by a flat curve with increasing surface roughness. The absorption by ice at  $\lambda = 1.64 \mu\text{m}$  decreases the value of the phase function in the forward scattering direction because of the decrease in the internal intensity. The phase function of cylindrical particles with a rough surface is close to a smooth phase function. Figure 2b shows the phase functions for the ellipsoidal particle  $r_{VA} = 50 \mu\text{m}$  at  $\lambda = 0.55 \mu\text{m}$  and  $1.64 \mu\text{m}$ . With increasing surface roughness, small peaks disappear and the phase functions at backscattering regions increase. The curve of these phase functions is similar to that of the Henyey-Greenstein phase function, in which these results are expected to simulate *HDRF* accurately (1).

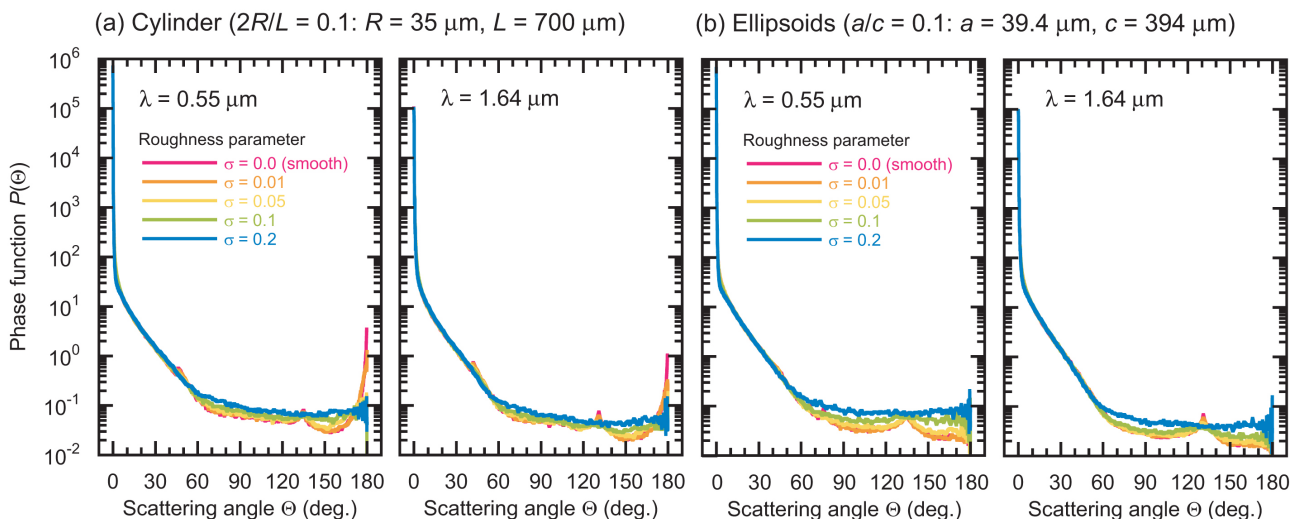


Figure 2: Change in phase function of (a) cylindrical and (b) ellipsoidal particles with surface roughness (roughness parameter from  $\sigma = 0.0$  to  $0.2$ ). Grain size is  $r_{VA} = 50 \mu\text{m}$ .

## RESULTS AND DISCUSSION

### HDRF measurements

Figure 3 shows the observed composite *HDRF* and normalized-*HDRF* (*N-HDRF*) for the two wavelengths using display methods (e.g. 19,20). The *N-HDRF*, which takes into account the *HDRF* at the nadir, is defined as

$$N - HDRF(\theta_o, \theta_v, \Delta\phi) = \frac{HDRF(\theta_o, \theta_v, \Delta\phi)}{HDRF(\theta_o, 0, \Delta\phi)}$$

The anisotropic reflection property is very significant at  $\lambda = 1.64 \mu\text{m}$ , while in the visible region at  $\lambda = 0.55 \mu\text{m}$ , the *N-HDRF* patterns are relatively flat. A similar result was obtained in the principal plane  $\Delta\phi = 0^\circ$  and  $180^\circ$  in measurements of anisotropic reflectance in Antarctica (19). These results were expected in view of the findings of (7) in which the *HDRF* pattern was found to be more anisotropic with a relatively strong forward peak for the near-infrared region, where snow is more

absorptive. The maximum value in the *N-HDRF* is observed at  $\theta_v = 85^\circ$  in the forward scattering direction ( $\Delta\phi = 0^\circ$ ). In the side-scattering direction ( $\Delta\phi = 90^\circ$ ), the *N-HDRF* decreases with the viewing angle  $\theta_v$  in the visible region, and increases in the near-infrared region. Comparing the *N-HDRF* between new and old snow, *N-HDRF* patterns of old snow are more anisotropic than those of new snow especially in the near-infrared region. A similar result was obtained in the visible region ( $\lambda = 0.5\text{--}0.6 \mu\text{m}$ ) (6).

(a) New snow: dendrites

(b) Old snow: granular snow

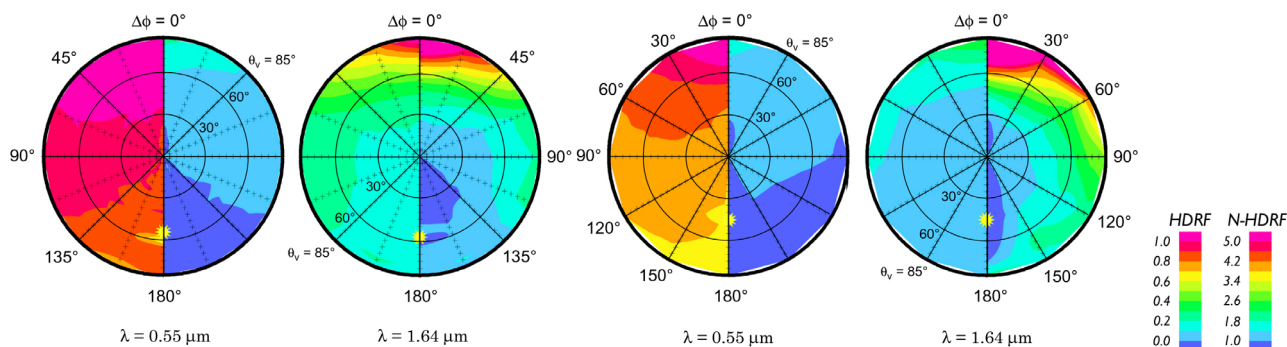


*Figure 3: Composite HDRF (left-half of each figure) and N-HDRF (right-half of each figure) of snow for two wavelengths as obtained from measurements of anisotropic reflectance: (a) new snow and (b) old snow. N-HDRFs are normalised by the value at the nadir. The plus signs on each HDRF and N-HDRF map indicate the observed points. The radial coordinate is proportional to the viewing angle  $\theta_v$ , which is zero at the centre of the circle (nadir) and is  $85^\circ$  on the circle. The illumination from the sun comes from the lower half of each map, indicated by the yellow mark. The top of each map is the forward scattering direction. The reflectance in the backscattering direction indicated by the yellow mark is low because of the detector shadow.*

### Theoretical calculation of HDRF and comparison with the measurement

The theoretical calculations of the *HDRF* and the *N-HDRF* are performed using different phase functions. The snow grain shape was assumed to be spherical, cylindrical, or ellipsoidal. The *HDRF* and *N-HDRF* are simulated for the smooth and rough ice particles, respectively. The roughness parameters are chosen to be  $\sigma = 0.1$ , where the tilt of the surface roughness is approximately between  $0^\circ$  and  $15^\circ$ . The aspect ratio of the cylindrical and ellipsoidal ice particles for new and old snow is set to  $2R/L = 0.1$  (column-like cylinder) and  $a/c = 1/3$  (prolate), respectively. The size of non-spherical ice particles could be represented by the equal  $V/A$ -sphere (12). Figures 4 and 5 show the theoretically calculated *HDRFs* and *N-HDRFs* for new and old snow, respectively. The most conspicuous difference between these *HDRFs* (*N-HDRFs*) is the presence of a rainbow at  $\lambda = 1.64 \mu\text{m}$  in the case of the spherical ice particles (Figures 4a and 5a). On the other hand, there is no rainbow at any wavelength in the *HDRF* (*N-HDRF*) measurements shown in Figure 3.

For the new snow (Figure 3a), the enhanced forward scattering peak ( $\Delta\phi = 0^\circ$ ) is clearly shown in measurements made at a large viewing angle, because the *HDRF* (*N-HDRF*) is very sensitive to the phase function (1). When the surface roughness is employed, the simulated *HDRFs* (*N-HDRFs*) using sphere decrease at the forward scattering direction and increase at the backscattering direction for any wavelengths, but still the rainbow effects remain on phase function (Fig. 4b). At  $\lambda = 0.55 \mu\text{m}$ , the simulated results of cylindrical particles with the smooth surface agree with the observed ones, except for high reflectance in the backscattering direction of  $(\theta_o, \phi_o) = (\theta_v, \phi_v)$  indicated by a yellow mark (Figure 4c). The high reflectance (peak) could be caused by a strong peak in the phase function of the scattering angle  $\phi \sim 180^\circ$  in the backscattering direction (see Figure 2a). If the surface roughness is employed in the single-scattering calculation, the high reflectance peak vanishes and the simulated *HDRF* (*N-HDRF*) patterns become consistent with the observed ones (Figure 4d). In the side-scattering direction ( $\Delta\phi = 90^\circ$  and  $270^\circ$ ), the reflectance at  $\Delta\phi = 90^\circ$  is the same as that at  $\Delta\phi = 270^\circ$ , the symmetry patterns at the side scattering direction are well simulated.

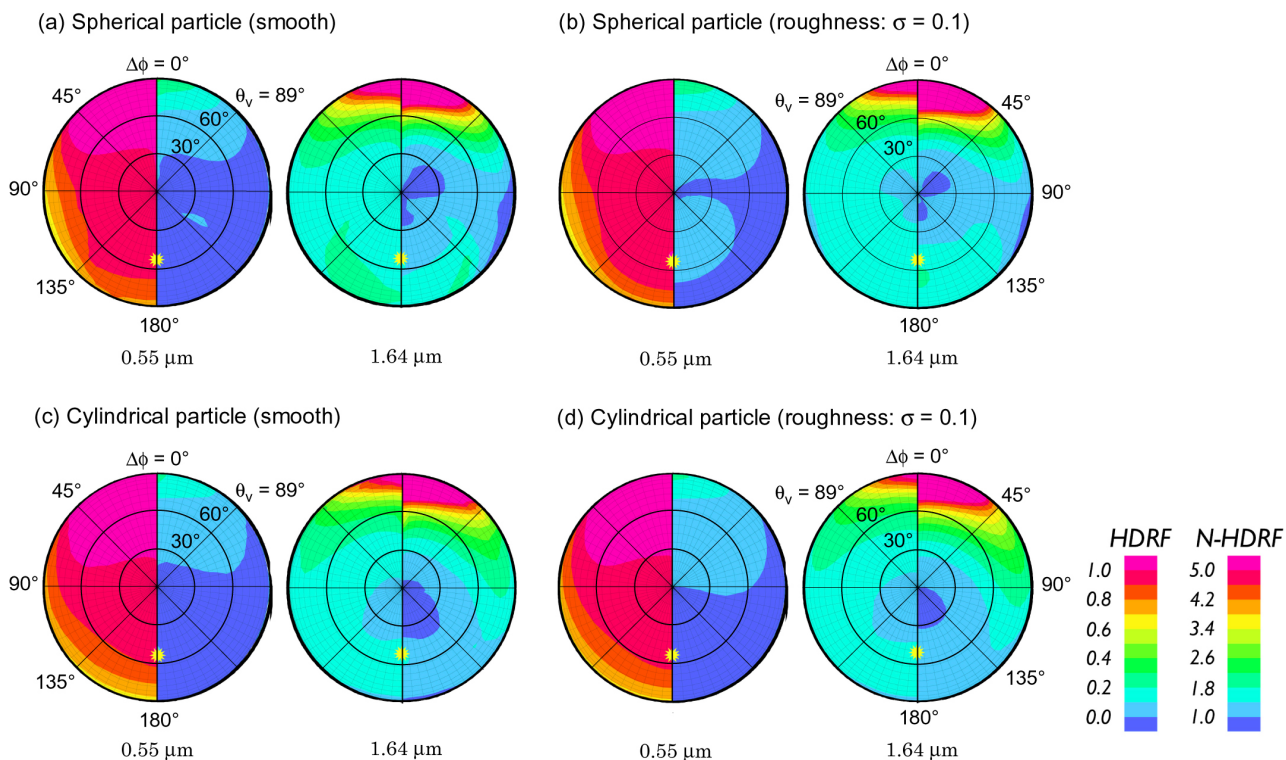


Figure 4: Theoretically calculated HDRFs (left-hand side) and N-HDRFs (right-hand side) of new snow for two wavelengths: (a,b) spherical and (c,d) cylindrical particles. Snow grain size is  $r_{VA} = 50 \mu\text{m}$ . The illumination from the sun comes from the lower direction of each map, indicated by a yellow mark.

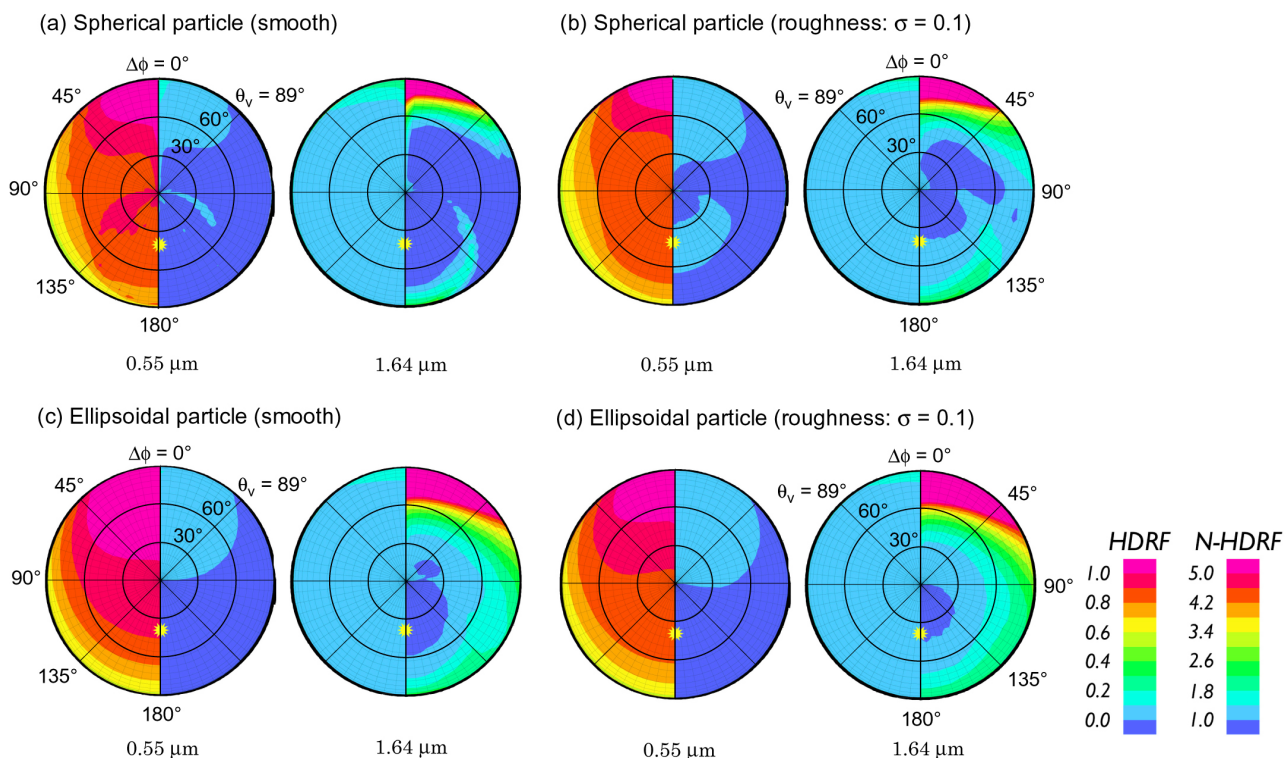


Figure 5: Same as Figure 4, but for old snow: (a,b) spherical and (c,d) ellipsoidal particles. Snow grain size is  $r_{VA} = 300 \mu\text{m}$ .

At  $\lambda = 1.64 \mu\text{m}$ , the theoretical HDRF (N-HDRF) patterns for cylindrical particles with smooth surface agree well with those of the measured ones except for the high reflectance in the backscattering

direction of  $(\theta_o, \phi_o) = (\theta_v, \phi_v)$  indicated by a yellow mark (Figure 4c) for the reason mentioned above. When employing surface roughness, the theoretical pattern for the cylindrical particle is roughly consistent with the measured one (Figure 4d). These comparisons between the simulated *HDRF*s and the measured ones indicate that the phase functions of the cylindrical particles with a rough surface simulate measurements of the *HDRF* better than those of a smooth surface.

For old snow, the simulated results of the spherical particles have some high peaks of the reflectance at any wavelength, because the curve of the phase function affects directly the *HDRF* patterns (1). For ellipsoidal particles, the simulated results are consistent with those of any viewing angle at  $\lambda = 0.55 \mu\text{m}$  (Figure 5c). When employing the surface roughness, the simulated *HDRF* (*N-HDRF*) patterns are flat for any wavelength (Figure 5d), but are not consistent with the observed ones in the forward scattering direction ( $\Delta\phi = 0^\circ$ ). Especially, the simulated *HDRF* values at  $\lambda = 1.64 \mu\text{m}$  are lower than the observed ones although the anisotropic reflection patterns in the forward scattering direction are well simulated. In the side-scattering direction ( $\Delta\phi = 90^\circ$  and  $270^\circ$ ), the *N-HDRF* patterns of the theoretical curves for non-spherical particles agree well with those of the measurement curve at any wavelength (Figure 5d). The comparison between the simulated and the observed *HDRF* (*N-HDRF*) patterns indicates that the optically equivalent snow grain size is predicted smaller than that of the granular snow observed by snow pit work. From the micrograph (not shown in this paper), the granular snow consists of clusters of grain and includes sun crust (melt freeze crust) in the surface layer. From the simulation results of single-scattering parameters of clusters of grain (17), the effect of clusters of grain on the *HDRF* could decrease the anisotropic reflection patterns in the forward scattering direction. Therefore, the sun crusts at surface layer may have produced the high *HDRF* (*N-HDRF*) values in the forward scattering direction.

## CONCLUSIONS

Radiative transfer models using non-spherical particles were developed to examine the effect of the snow grain shape on the angular distribution of snow reflectance. In these models, snow grain shapes are assumed to be cylindrical for new snow and ellipsoidal for old snow, because the optically equivalent grain size is not the size of entire snow crystals but the branch width of dendrites or diameter of individual grains for granular snow (1). For representing natural ice crystals, surface roughness is added to the single-scattering calculation which is derived by ray-tracing (14). For the validation of these models, observations of the *HDRF* were carried out for new snow on February 2001 and for old snow on March 2004 in the flat snowfield of Hokkaido, Japan. For the new snow, the snow surface was covered by dendrites and second layers, which mainly consisted of faceted crystal and depth hoar. Most of the old snow layers consisted of granular snow. The snow surface was partially covered by sun crust (melt freeze crust).

The results of *HDRF* measurements show that the anisotropic reflection patterns were significant in the near-infrared region while the visible *HDRF* patterns were relatively flat for both snows. These patterns were consistent with previous studies (e.g. 1,4). Comparisons of the theoretically calculated *HDRF* and the observed one show that the simulated *HDRF* using cylindrical particles combined with the surface roughness as surrogate for new snow are consistent with the observed ones. This means that a smooth phase function is more suitable than the Mie phase function for the *HDRF* calculation of new snow because the curve of the phase function directly affects the *HDRF* patterns. From this point of view, it seems that general hexagonal shapes as surrogates for general snow are not suitable for *HDRF* calculation because the halo is not usually seen on the snow surface.

For old snow, the results obtained using ellipsoidal particles in the visible region are consistent with the observed ones. However, in the near-infrared region the observed *HDRF* is relatively higher than the simulated one especially in the forward scattering direction. This means that the optically equivalent snow grain size could be smaller than the actual size. From the micrograph (not shown in this paper), the granular snow consists of clusters of grain and includes sun crust. Thus, the sun crusts at the surface layer may have produced the high *HDRF* values in the forward scattering direction because the *HDRF* at near-infrared region could be sensitive to the surface structure of

snow. For the radiative transfer calculation of old snow, the effect of the sun crusts on the *HDRF* under various geometric conditions needs to be further considered.

## ACKNOWLEDGEMENTS

This work was supported by Research Fellowships of the Japan Society for the Promotion of Science for Young Scientists. It was conducted as part of the ADEOS-II/GLI Cal/Val experiments supported by the Japan Aerospace Exploration Agency.

## REFERENCES

- 1 Aoki Te, Ta Aoki, M Fukabori, A Hachikubo, Y Tachibana & F Nishio, 2000. Effects of snow physical parameters on spectral albedo and bi-directional reflectance of snow surface. Journal of Geophysical Research, 105: 10219-10236
- 2 Tanikawa T, Te Aoki & F Nishio, 2002. Remote sensing of snow grain size and snow impurities from Airborne Multispectral Scanner data using a snow bidirectional reflectance distribution function model. Annals of Glaciology, 34: 74-80
- 3 Leroux C, J Deuzé, P Goloub, C Sergent & M Fily, 1998. Ground measurements of the polarized bidirectional reflectance of snow in the near-infrared spectral domain: Comparisons with model results. Journal of Geophysical Research, 104: 31697-31709
- 4 Painter T H & J Dozier, 2004. Measurements of the hemispherical-directional reflectance of snow at fine spectral and angular resolution. Journal of Geophysical Research, 109: doi:10.1029/2003JD004458
- 5 Kuhn M, 1985. Bidirectional reflectance of polar and alpine snow surface. Annals of Glaciology, 6: 164-167
- 6 Steffen K, 1987. Bidirectional reflectance of snow at 500-600 nm. In: Large Scale Effects of Seasonal Snow Cover, edited by B Goodison, R G Barry & J Dozier, 436 pp. IAHS Publication Series, 166: 415-425
- 7 Warren S G, R E Brandt & P O'Rawe Hinton, 1998. Effect of surface roughness on bidirectional reflectance of Antarctic snow. Journal of Geophysical Research, 103: 25789-25807
- 8 Greuell W & M de Ruyter de Wildt, 1999. Anisotropic reflection by melting glacier ice: Measurements and parametrizations in Landsat TM Bands 2 and 4. Remote Sensing of Environment, 70: 265-277
- 9 Bourdelles B & M Fily, 1993. Snow grain-size determination from Landsat image over Terre Adélie, Antarctica. Annals of Glaciology, 17: 86-92
- 10 Fily M, B Bourdelles, J P Dedieu & C Sergent, 1997. Comparison of in situ and Landsat Thematic Mapper derived snow grain characteristics in the Alps. Remote Sensing of Environment, 59: 452-460
- 11 Nolin A W & J Dozier, 2000. A hyperspectral method for remotely sensing the grain size of snow. Remote Sensing of Environment, 74: 207-216
- 12 Grenfell T C & S G Warren, 1999. Representation of a nonspherical ice particle by a collection of independent spheres for scattering and absorption of radiation. Journal of Geophysical Research, 104(D24): 31697-31709
- 13 Aoki Te, Ta Aoki, M Fukabori & A Uchiyama, 1999. Numerical simulation of the atmospheric effects on snow albedo with a multiple scattering radiative transfer model for the atmosphere-snow system. Journal of the Meteorological Society of Japan, 77: 595-614

- 14 Macke A & M I Mishchenko, 1996. Applicability of regular particles shapes in light scattering calculations for atmospheric ice particles. Applied Optics, 35: 4291-4296
- 15 Takano Y & K N Liou, 1995. Radiative transfer in cirrus clouds. III. Light scattering by irregular ice crystals. Journal of Atmospheric Science, 52: 818-837
- 16 Yang P & K N Liou, 1998. Single-scattering properties of complex ice crystals in terrestrial atmosphere. Contributions to Atmospheric Physics, 71(2): 223-248
- 17 Tanikawa T, Te Aoki, M Hori, A Hachikubo, O Abe & M Aniya, 2006. Monte Carlo simulations of spectral albedo for artificial snowpacks composed of spherical and non-spherical particles. Applied Optics (in press)
- 18 Mishchenko M I & A Macke, 1999. How big should hexagonal ice crystals be to produce halos? Applied Optics, 38: 1626-1629
- 19 Taylor V R & L L Stowe, 1984. Reflectance characteristics of uniform earth and cloud surfaces derived from Nimbus 7 ERBE. Journal of Geophysical Research, 89: 4987-4996
- 20 Carlson R W & T Arakelian, 1993. Spectral bidirectional reflectance and energy absorption rates of Antarctic snow. Antarctic Journal of the U. S., 28: 256-258